Electrokinetic Instabilities and Sample Stacking

H. Lin, M.H. Oddy and J.G. Santiago

Mechanical Engineering Department, 530-224, 440 Escondido Mall
Stanford University, Stanford, CA 94305, USA, juan.santiago@stanford.edu

ABSTRACT

Electrokinetic instabilities occur in electrokinetic microchannel flows with heterogeneous electrolytes. These instabilities can be leveraged in providing rapid mixing, but are often unwanted in microfluidic applications which use heterogeneous electrolytes to achieve high resolution and new functionality. One important application of heterogeneous electrolytes is field-amplified sample stacking methods which use conductivity gradients to achieve sample preconcentration prior to electrophoretic separation. In this work, we analyze the flow physics of electrokinetic flows with conductivity gradients using theoretical analyses, numerical computations, and experimental observations. Various models including two-dimensional and depth-averaged formulations have been developed, and modeling results compare well with experimental observations. Based on this understanding, we have developed novel sample stacking methods with sample preconcentrations exceeding 1,000 fold. The work also provides guidelines for the design and optimization of on-chip chemical and bio-analytical assays.

Keywords: electrokinetic instability, electric conductivity gradient, sample stacking, micromixing

1 INTRODUCTION

Over the past decade there has been extensive research into the design of devices that perform chemical analyses in micro-fabricated fluidic channel structures. Many of these devices apply electrokinetic liquid-phase, bioanalytical techniques such as capillary electrophoresis and isoelectric focusing, and often manipulate samples having poorly characterized or unknown electrical conductivities. As a result, conductivity mismatches often occur between the sample/reagent species and the background electrolyte. In the presence of applied electric fields conductivity gradients can induce electromechanical coupling and complex, unstable flow behavior. These instabilities often compromise desired sample control and pose significant challenges for a wide class of on-chip processes.

In 2001 Oddy *et al.* first reported observation of electrokinetic instability (EKI) in a micro-capillary (Oddy *et al.*, 2001). In a slightly different geometry (microfluidic T-junction), Chen and Santiago also reported spatial amplification of disturbances which was later identified as convective instability (Chen and Santiago, 2002; Chen *et al.*, 2005). In both of the experiments critical applied electric field strengths existed above which instabilities and significant stirring occurred.

Following these initial experimental observations, there has been a development of models for electrokinetic flow instabilities. Lin *et al.* (2004) and Chen *et al.* (2005) developed a generalized EHD modeling framework for the study of flow instabilities in electrokinetic microsystems with high-conductivity electrolyte. These models for electrokinetic flow instabilities were derived from the so-called "leaky dielectric" concept first developed by Melcher and Taylor (1969), Hoburg and Melcher (1976), and Baygents and Baldessari (1998). The various linear analyses and nonlinear simulations by Lin *et al.* and Chen *et al.* reproduced instability dynamics and provided good qualitative and quantitative agreement with experimental observations. Using a convective framework, Chen *et al.* (2005) also showed that EKI can manifest itself convectively in the presence of a strong electroosmotic flow, and have identified both convectively and absolutely unstable eigenvalues in their analyses. More recently, Storey *et al.* (2005) and Lin *et al.* (2005) presented depth-averaged versions of the governing equations used by the Lin *et al.* (2004) model. Their model results compared favorably with a complete three-dimensional computation for thin microchannel geometries but at much reduced computational costs.

In this paper we present our experimental, analytical, and computational results of modeling and understanding of EKI in electrokinetic microchannels. Based on the understanding, and by avoiding EKI, we are implementing novel chip designs to achieve high ratio sample preconcentration.

2 EXPERIMENAL RESULT

In Figure 1 we show a few example results from our experiments (Lin *et al.,* 2004). The microchannel consisted of a borosilicate glass capillary (Wilmad-Labglass, NJ) with a rectangular cross-section. The channel was 4 mm long (streamwise direction), 1 mm wide (spanwise direction), and 0.1 mm deep (depth direction). Two buffer streams (50 μS/cm, shown in *red*; and 5 μS/cm, shown in *blue*; Figure 1) initially occupied the upper and lower halves of the microchannel resulting in a diffuse conductivity gradient along the spanwise direction; an electric field was subsequently applied along the streamwise direction. The imposed electric potential initiated an electroosmotic flow in the channel and, for

electric fields above a threshold value, electrokinetic instabilities.

A representative set of images from experiments conducted at 25,000, 50,000 and 75,000 V/m of applied electric fields are shown in Figure 1. In each case, the top figure of each series shows the initial, undisturbed conductivity interface ($t = 0$). For an applied field of 25,000 V/m, the interface was only slightly perturbed and only slight fluctuations are apparent in the images captured at 4.0 s and 5.0 s. At the two higher applied voltages, the interface exhibited a rapidly-growing wave pattern within the first 1 s. The transverse and fluctuating velocities associated with this unstable motion resulted in rapid mixing of the two streams. At the 75,000 V/m applied field, the channel reached a well-stirred state with nearly-homogeneous concentration fields observable within 5 s.

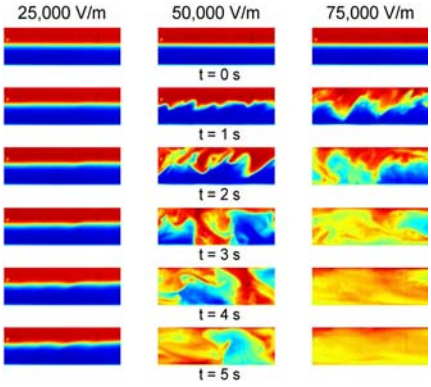

Figure 1. Instability mixing of high (*red*) and low conductivity (*blue*) streams. Results are shown for applied fields of 25,000, 50,000, and 75,000 V/m and at various times. The electric field (applied at $t = 0$ s) and bulk flow directions were from left to right. Each image corresponds to a physical area 1 mm wide and 3.6 mm long.

3 FORMULATION AND 2D ANALYSIS

To study the instability we use a general framework derived from the conservation laws for a dilute, two-species electrolyte solution (Probstein, 1994). We have adopted (with justification) a relaxation assumption to simplify the equations. The scaling analysis and derivations are discussed in detail in Lin *et al.* (2004) and are not repeated here. The (*dimensionless*) equations read

$$\frac{\partial \sigma}{\partial t} + \mathbf{v}\cdot\nabla\sigma = \frac{1}{Ra_e}\nabla^2\sigma, \tag{1}$$

$$\nabla\cdot(\sigma\nabla\Phi) = 0, \qquad \nabla^2\Phi = -\rho_E, \tag{2}$$

$$\nabla\cdot\mathbf{v} = 0 \tag{3}$$

$$Re\left(\frac{\partial \mathbf{v}}{\partial t} + \mathbf{v}\cdot\nabla\mathbf{v}\right) = -\nabla p + \nabla^2\mathbf{v} - \rho_E\nabla\Phi, \tag{4}$$

where σ is the conductivity, $\mathbf{v}$ is the bulk fluid velocity, and Φ is the electric field including both applied and generated components. The electric Rayleigh number Ra_e is similar to a Peclet number and represents the importance of molecular diffusion and electric-body-force driven convection. Both the Rayleigh and the Reynolds numbers are defined with the so-called electroviscous velocity, a velocity scale derived by setting equal the electric body force and the viscous force in the momentum equation (Hoburg and Melcher, 1976; Lin *et al.*, 2004; Chen *et al.*, 2005).

We first present a model where we assume that the flow exists *only* in the streamwise-spanwise plane, and that there are no dynamics in the (thin) depth direction. We use a temporal linear stability analysis to predict the regimes where we expect instability to occur. In Figure 2 we show the contours of dimensional growth rate s in the parameter space of wave number k and Rayleigh number. The dimensional applied field is provided on the right axis. The neutral stability curve is obtained by setting $s = 0$. A threshold electric field is successfully captured from the minimal value of E_o on the neutral stability curve. As originally reported by Baygents and Baldessari (1998), we found that the inclusion of the diffusive term $\nabla^2\sigma/Ra_e$ in equation (1) is crucial for the existence of the neutral stability curve.

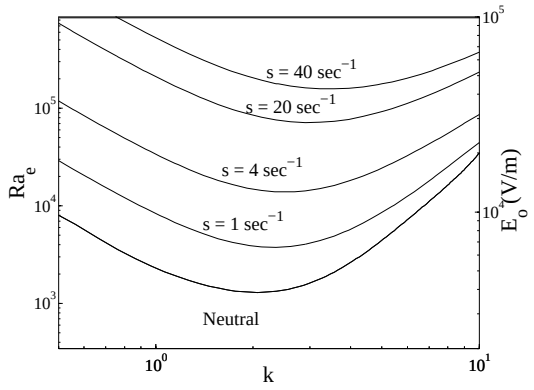

Figure 2. Contour plot of growth rates (s) versus wave number and Rayleigh number. Dimensional applied electric field is provided on the right axis. For the case plotted here, the ratio of the conductivity between the two streams is 10.

We have also solved the two-dimensional governing equations (1-4) numerically to capture the nonlinear evolution of the instability observed in the experiments. The solution details are documented in Lin *et al.* (2004), and the results are shown in Figure 3. The model reproduces many of the essential features observed in the experiments, including the shape and initial break-up dynamics of the interface, the transverse growth of a wave pattern in the interface, and the roll-up of scalar structures observed at later times. Note the similarity in the most unstable and apparent wave number at later times between the simulation and experiments.

Despite similarities between wave numbers and the dynamics of the interface breakup, discrepancies exist

between the quantitative predictions of the model and the experimental observations. For example, Figure 2 predicts a threshold field around 4,000 V/m, much lower than the value of approximately 30,000 V/m determined from the set of experiments shown in Figure 1. Furthermore, the nonlinear simulations from the two-dimensional model (Figure 3) only reproduce experimentally observed instability dynamics at much lower field strengths (10,000, 17,500, and 25,000 V/m) when compared with those used in experiments (25,000 V/m, 50,000 V/m, and 75,000 V/m, Figure 1). The reason for this is further discussed in the next section.

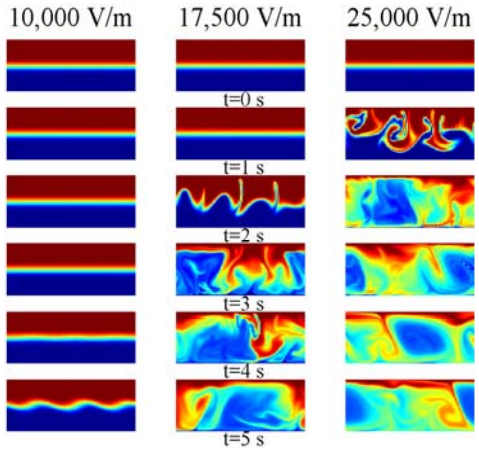

Figure 3. Instantaneous images of the simulated instability at various instances in time for different driving electric fields. In this color scheme red corresponds to the high conductivity buffer, and blue to the low one. The image corresponds to a physical domain of $3.6\text{mm} \times 1\text{mm}$. The time for noticeable waves to develop is decreased as the field is increased.

4 DEPTH-AVERAGED MODEL AND SAMPLE STACKING

In the previous sections we have provided a two-dimensional framework that captures the primary physics of the instability flow. However, a neglect of the flow physics in the thin depth direction has also led to inaccuracies in the quantitative model predictions, and in general three-dimensional flow physics in the microchannels has to be modeled in order to achieve quantitative flow predictions (Lin *et al.,* 2004). However, an alternative to full three-dimensional simulations is a depth-averaged approach which has been shown to lead to accurate model predictions at reduced computational cost (Lin *et al.*, 2005; Storey *et al.,* 2005; Chen *et al.,* 2005).

Here we follow the approach of Lin *et al.* (2005) and briefly elucidated the depth-averaged method. We perform a complete asymptotic analysis of the full three-dimensional equations (1-4) based on a smallness parameter δ; here $\delta \equiv d/H$ is the small channel depth-to-width aspect ratio. Our general methodology follows a combined lubrication (for the momentum equations) and Taylor-Aris (for the convective-diffusion of the conductivity field) theory. Without presenting the details of the derivation (documented in Lin *et al.,* 2005), we list the final equations as

$$\frac{\partial \overline{\sigma}}{\partial t} + \overline{\mathbf{u}} \cdot \nabla_H \overline{\sigma} = \frac{1}{Ra_e}\left\{ \nabla_H^2 \overline{\sigma} + \frac{2}{105} Ra_e^2 \delta^2 \nabla_H \cdot [\overline{\mathbf{U}}(\overline{\mathbf{U}} \cdot \nabla_H \overline{\sigma})] \right\}, \tag{5}$$

$$\nabla_H \cdot (\overline{\sigma} \nabla_H \overline{\Phi}) = 0, \qquad \nabla_H \cdot \overline{\mathbf{u}} = 0, \tag{6}$$

$$Re\delta^2 \left(\frac{\partial \overline{\mathbf{u}}}{\partial t} + \overline{\mathbf{u}} \cdot \nabla_H \overline{\mathbf{u}} \right) = -\nabla_H \overline{p} + \nabla_H^2 \overline{\Phi} \nabla_H \overline{\Phi} - 3\overline{\mathbf{U}} + \delta^2 \nabla_H^2 \overline{\mathbf{u}}. \tag{7}$$

Here the overbar denotes a depth-averaged quantity, the operator ∇_H denotes the in-plane gradient (to distinguish from the full three-dimensional gradient), and $\overline{\mathbf{U}} \equiv \overline{\mathbf{u}} - \mathbf{u}_{eo}$ is the difference between the total depth-averaged velocity and the electroosmotic velocity.

The main contributions of this work is that we have reduced the original full three dimensional equations (1-4) to the quasi-two-dimensional equation set (5-7), in which flow physics in the depth direction manifest themselves as additional terms (*e.g.* the two-dimensional Taylor dispersion term in equation (5), and the DBF momentum equation (7)) in an otherwise two-dimensional formulation. Through this formulation we can achieve the accuracy of full three-dimensional modeling at the expenses of two-dimensional computations.

Using this depth-averaged framework we have reproduced the experimental image presented in Figure 1 at the two lower voltages (25,000 and 50,000 V/m); the result is shown in Figure 4. Again the model reproduces essential features observed in the experiments such as fastest growing wave numbers and the growth rates of the interface disturbance amplitude. However, note that the computations are now at exactly the same field strength as those applied in the experiments (as opposed to the unnaturally lower fields used for comparison with the simple 2D model results of Figure 3).

The depth-averaged equation set (5-7) has also been developed to be applicable to generalized electrokinetic flows with heterogeneous conductivity configuration. We are applying the depth-averaged model to the study of dynamics and optimization of capillary electrophoresis separations where sample is preconcentrated in using field-amplified-sample-stacking (FASS). Figure 5 shows a simulation of a FASS configuration where a sample analyte is injected into a separation microchannel as a finite injection plug (*i.e.*, an initial top hat distribution along the channel axis). We compare with three-dimensional direct numerical simulations (where the flow physics in the depth direction is directly computed rather than modeled) the results from the depth-averaged model. The comparison yields good agreement.

In the FASS flow field of Figure 5, axial conductivity gradients lead to strong axial gradients in electric field magnitude. This coupling of electric and conductivity fields leads to both electric body forces in the bulk and strong gradients in electroosmotic velocity near the wall. The dispersion of the (initially blue) analyte region here is dominated by gradients in electroosmotic velocity and not electrokinetic flow instabilities. In fact, we find that the flow is stable for fields as high as 1.25 kV/cm in this FASS flow in a 100 by 10 μm channel. This has led us to the preliminary conclusion that configurations with collinear electric field and conductivity gradients (as in FASS) are much more stable than configurations with a significant angle between these two vector quantities. We are currently working on several novel chip geometries and injection methods to achieve high-ratio sample preconcentration. One example is chips with *in situ* polymerized porous regions designed to both aid in pressure-driven sample injections and avoid electrokinetic instabilities; the best achieved stacking ratio in this design is more than 1,000 fold (Jung *et al.,* 2003). We are currently testing chip devices designed to achieve 10,000 fold sample concentration increases.

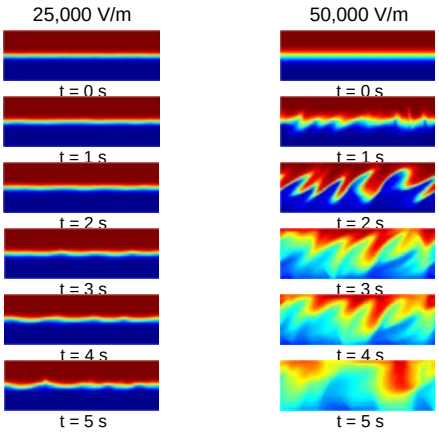

Figure 4. Nonlinear simulation using the quasi-two-dimensional, depth-averaged equations (5-7) which include flow physics in the depth direction. The results accurately reproduce the experimental observations (Figure 1) at the same applied electric fields.

5 CONCLUSIONS AND FUTURE WORK

We have presented experimental, numerical, and analytical results that explain the basic mechanisms behind an electrokinetic mixing phenomenon observed in microfluidic channels. We have presented various analysis and numerical simulations, and successfully captured qualitative as well as quantitative features of observed flow fields. In particular, our depth-averaged model is able to achieve the accuracy of full three-dimensional computations with a quasi-two-dimensional set of equations. This reduced, two-dimensional computational cost is particularly advantageous in future investigations such as optimization study. Based on our understanding of the instability, we have also been able to avoid EKI and demonstrate high stacking ratio in sample stacking experiments.

This work was sponsored by DARPA (Contract Number F30602-00-2-0609) with Dr. Anantha Krishnan as contract monitor and by an NSF PECASE Award (J.G.S., CTS-0239080-001) with Dr. Michael W. Plesniak as contract monitor.

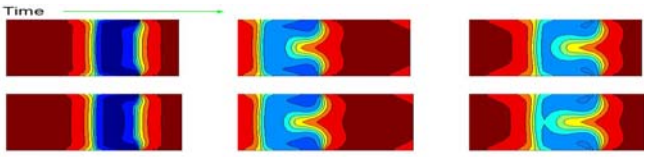

Figure 5. Depth-averaged simulation of FASS-type flow (top row) and comparison with 3D DNS (bottom row). Here blue denotes low conductivity and red denotes high conductivity. The electric field is applied in the streamwise direction. For further details see Lin *et al.* (2005).

REFERENCES

Baygents, J., and Baldessari, F., 1998, Electrohydrodynamic instability in a thin fluid layer with an electrical conductivity gradient, *Phys. Fluids* **10**(1), 301-311.

Chen. C.-H., and Santiago, J. G., 2002, Electrokinetic instability in high concentration gradient microflows, *Proceedings of IMECE-2002*, CD vol. 1, #33563.

Chen, C.-H., Lin, H., Lele, S. K., and Santiago, J. G., 2005, Convective and absolute electrokinetic instability with conductivity gradients, *J. Fluid Mech.*, **524**, 263-303.

Hoburg, J. F., and Melcher, J. R., 1976, Internal electrohydrodynamic instability and mixing of fluids with orthogonal field and conductivity gradients, *J. Fluid Mech.* **73**, 333.

Jung, B., Bharadwaj, R., and Santiago, J.G., 2003, Thousandfold signal increase using field-amplified sample stacking for on-chip electrophoresis, *Electrophoresis* **24**, 3476.

Lin, H., Storey, B.D., and Santiago, J.G., 2005, A depth-averaged electrokinetic flow model for thin microchannels, *Proc. Roy. Soc. A.*, submitted.

Lin, H., Storey, B. D., Oddy, M. H., Chen, C.-H., and Santiago, J. G., 2004, Instability of electrokinetic microchannel flows with conductivity gradients, *Phys. Fluids* **16**(6), 1922-1935.

Melcher, J. R., and Taylor, G. I., 1969, Electrohydrodynamics: a review of the role of interfacial stresses, *Annu. Rev. Fluid. Mech.* **1**, 111-146.

Oddy, M.H., Santiago, J.G., and Mikkelson, J.C., 2001, Electrokinetic instability micromixing, *Anal. Chem.* **73**, 5822-5832.

Probstein, R. F., 1994, *Physicochemical Hydrodynamics*, John Willey & Sons, New York.

Storey, B. D., Tilley, B. S., Lin, H., and Santiago, J. G., 2005, Electrokinetic instabilities in thin microchannels, *Phys. Fluids*, **17**(1), ref #018103.